Available online at www.sciencedirect.com
ScienceDirect
Journal of Bionic Engineering 11 (2014) 497–505

An Experimental Analysis of Overcoming Obstacle in Human Walking

Tao Li[1], Marco Ceccarelli[2], Minzhou Luo[1], Med Amine Laribi[3], Said Zeghloul[3]

1. *Institute of Advanced Manufacturing Technology*, *Hefei Institutes of Physical Science*, *Chinese Academy of Sciences*, *Changzhou* 213164, *P. R. China*
2. *Laboratory of Robotics and Mechatronics*, *University of Cassino and South Latium*, *Cassino* 03043, *Italy*
3. *Institute PPRIME - DGMSC*, *CNRS-University of Poitiers - ENSMA*, 15 *Rue de l'Hôtel Dieu*, 86000, *Poitiers*, *France*

Abstract

In this paper, an experimental analysis of overcoming obstacle in human walking is carried out by means of a motion capture system. In the experiment, the lower body of an adult human is divided into seven segments, and three markers are pasted to each segment with the aim to obtain moving trajectory and to calculate joint variation during walking. Moreover, kinematic data in terms of displacement, velocity and acceleration are acquired as well. In addition, ground reaction forces are measured using force sensors. Based on the experimental results, features of overcoming obstacle in human walking are analyzed. Experimental results show that the reason which leads to smooth walking can be identified as that the human has slight movement in the vertical direction during walking; the reason that human locomotion uses gravity effectively can be identified as that feet rotate around the toe joints during toe-off phase aiming at using gravitational potential energy to provide propulsion for swing phase. Furthermore, both normal walking gait and obstacle overcoming gait are characterized in a form that can provide necessary knowledge and useful databases for the implementation of motion planning and gait planning towards overcoming obstacle for humanoid robots.

Keywords: human locomotion, overcoming obstacle, walking gait, biped robot, motion capture

doi: 10.1016/S1672-6529(14)60062-7

1 Introduction

In recent years, research works on humanoid robots have been growing rapidly. Human locomotion provides a perfect source of inspiration for the research and development of humanoid robots because nature has solved admirably the problem of biped locomotion during a long time evolution of human beings. In general, human walking has several main characteristics: first, it is fairly smooth because the Center of Gravity (COG) of the upper body has minor motion in the vertical direction; second, it is quite efficient because human beings can make use of gravity effectively[1,2] and the energy that is needed during walking is quite low; and third, it can be considered as optimal for energy consumption[3]. These characteristics are just the desired targets for researchers who are developing humanoid robots.

Since humanoid robots are designed to work in unconstructed environments, researchers have proposed many strategies for biped robots to move in unpredictable environments or on rough terrain[4–6]. Besides, the environments are usually cluttered with unavoidable obstacles, thus the robots should also be able to overcome them. Human beings can know whether we can overpass an obstacle by intuition or experience. However, robots do not have such abilities. Thus, suitable methods should be developed to perform obstacle overcoming for robots. Guan *et al*. analyzed the feasibility for humanoid robots to overcome given obstacles by taking into account the constraints of collision-free, balance and kinematics[7]. However, they just focused on quasi-static stepping over by keeping the projection of the global COG of the robot within the polygon of support, which resulted in somehow unnatural slow motions. Verrelst *et al*. extended the work and proposed fluent dynamic motion using stability criteria on Zero Moment Point (ZMP) instead of COG[8]. Nevertheless, characteristics of human obstacle overcoming behavior have not been taken into account in those works. It is believed that studying obstacle overcoming behavior in

Corresponding author: Marco Ceccarelli
E-mail: ceccarelli@unicas.it

human locomotion will bring us more inspirations for the research and development of robots that can overcome obstacle.

Human locomotion has been widely studied by researchers with the aim to develop humanoid robots[9–13]. In particular, human obstacle overcoming has been widely studied. Draganich and Kuo reported their comparative analysis on the effects of walking speed on obstacle crossing in healthy young and healthy older adults[14]. Krell and Patla analyzed the influence of multiple obstacles in the travel path on avoidance strategy[15]. Chou *et al* investigated motion of the whole body's center of mass when stepping over obstacles of different heights[16]. Lowrey *et al* described age-related changes in avoidance strategies when negotiating single and multiple obstacles in their work[17]. Patla and Vickers studied where and when do we look as we approach and step over an obstacle in the travel path[18]. Later in 2006, Patla and Greig reported their findings believing in that successful obstacle negotiation needs visually guided on-line foot placement regulation during the approach phase[19]. Meanwhile, MacLellan and Patla announced their work on stepping over an obstacle on a compliant travel surface, and revealed adaptive and maladaptive changes in locomotion patterns[20]. These works give an insight view of human obstacle overcoming. However, they were carried out with the aim to provide database for rehabilitation, surgery and psychology. Most of the results cannot be used as reference knowledge for the research and development of biped robots.

The target and originality is to study human locomotion, especially to analyze and characterize human obstacle overcoming, with the aim to provide reference knowledge for the research and development of biped robots. Hence Vicon Nexus[21], which is a commercial motion capture platform, has been used to analyze the operation of overcoming obstacle in human walking. In particular, kinematics of human locomotion in terms of trajectory, velocity, acceleration, and joint variation has been investigated; ground reaction force has been measured; modeling and characterization of both normal walking gait and obstacle overcoming gait have been implemented.

2 An experimental layout

Fig. 1a depicts a scheme of Vicon Nexus motion capture system, which is mainly composed of MX cameras (a), acquisition platform units (b), a PC with Nexus software (c), and MX cables (d). Furthermore, with the aim to measure ground reaction force, six force plates (e: 1–6) are used. The force plates are the products of KISTLER Ltd., which have extremely wide measuring range, excellent measuring accuracy, high natural frequency, versatility, and threshold F_z <50 mN. Furthermore, this force plate is designed specifically for use in basic research, sports and gait analysis. The plate can be mounted in any position. Moreover, a video recorder (f) is used in the system to record the process of the experiment. In addition, an experimental subject with markers is essential (g). Using Nexus software, x, y and z coordinates of each marker at each moment are recorded in a reference coordinates frame.

Fig. 1b shows an experimental setup according to Fig. 1a. In the experiment, 10 MX cameras were used to achieve quite accurate results. In the middle part of the walking platform, 6 force sensors, which can provide 6D interaction wrench measurements, were installed for

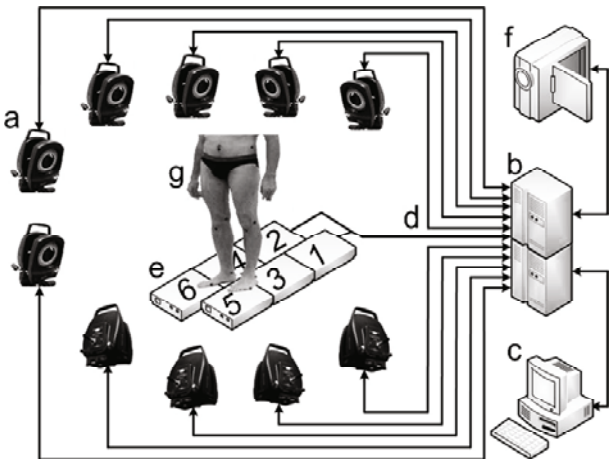

(a)

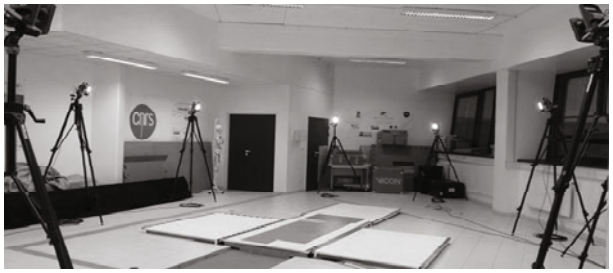

(b)

Fig. 1 A scheme of Vicon Nexus[13]: (a) a-10 MX cameras; b-acquisition platform units; c-PC with Nexus software; d-MX cables; e-6 force plates; f-classical camera recorder; g-subject with markers; (b) an experimental setup of the motion capture system.

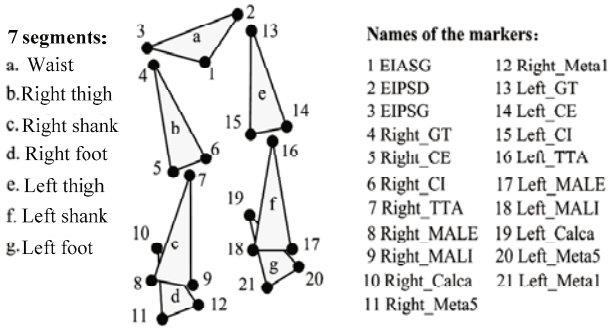

Fig. 2 Used marker configuration for the lower body for lab experiments of Fig. 1a frame.

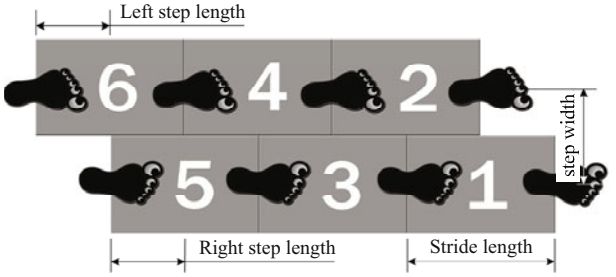

Fig. 3 Gait planning for measuring ground reaction force during the first test (1-6: six force plates).

measuring ground reaction forces. The marker configuration is shown in Fig. 2. The lower body was divided into 7 segments, which are the waist, left thigh, left shank, left foot, right thigh, right shank, and right foot. In order to obtain the orientation between different segments, at least 3 markers were pasted on each segment. Thus, total 21 markers were used. In particular, markers 4 and 13 were placed at the hip joints, 7 and 16 were placed at the knee joints, 8 and 17 were placed at the ankle joints, 10 and 19 were placed at the heels, 11 and 20 were placed at the toe joints.

With the abovementioned experimental setup, two experiments of straight walking and obstacle overcoming were carried out. Each experiment was carried out with 6 people with different height and weight; and for each person, each type of experiment was carried out for 3 times. We utilized people with different height and weight because we wanted to find out that if people's walking gait is under the influence of their height and weight. We utilized a group of people because we wanted to make the experiments impersonal and reliable. The straight walking experiment was performed especially for measuring the ground reaction force, whereas the obstacle overcoming experiment was carried out with the aim to characterize the walking gait. Frequency of the MX cameras was set up to 200 Hz, which means each camera records 200 frames per second. The subject for this experiment was a normal adult man, who was 1.70 m high and weight 62 kg. Walking velocity of the subject was not specified but walking at a normal speed and it can be measured during the experiments.

In the first test, the ground reaction forces were measured by 6 force plates. Walking steps are depicted in Fig. 3. The detailed process is as follows: first, the left foot strikes the sixth force plate with its toe joint, then the right foot strikes the fifth force plate with its toe joint, and then the left foot lands on the sixth and the fourth plates with its heel and toe joint sequentially. The following steps are similar as the first two steps. Stride length is the distance travelled by a person during one stride, and it can be measured as the length between two adjacent heel strikes on the same foot. With normal subjects, left step length plus right step length make one stride length. As shown in Fig. 3, stride length is nearly equal to the length of one force plate, and step width is equal to the width of the one force plate. Left and right step lengths, stride length and step width are illustrated in Fig. 3 with average measures of 0.6 m, 1.2 m, and 0.2 m, respectively.

In the second test, namely the phase of obstacle overcoming, a cuboid was placed in front of the subject. Length, width and height of the cuboid are 0.1 m, 0.5 m, and 0.25 m, respectively. Fig. 4a shows a sequence of photos of the experiment. After the experiment was implemented, two kinds of information were obtained: first, the whole experimental process recorded by Vicon Nexus software; and second, video recorded by the classical camera recorder (as shown in Fig. 1a). With these kinds of information, post-processing was carried out with the following two steps.

The first step of post-processing is to check if each marker has been recognized successfully and continuously by the MX cameras through the whole process. If so, an excel file which contains the data of coordinates of each maker can be outputted; if not, it means some positions has not been recognized and recorded by the system, namely there are gaps existing in the trajectory of the marker, in this case proper treatment need to be carried out with the aim to fill those gaps to make each maker has a continuous trajectory through the whole

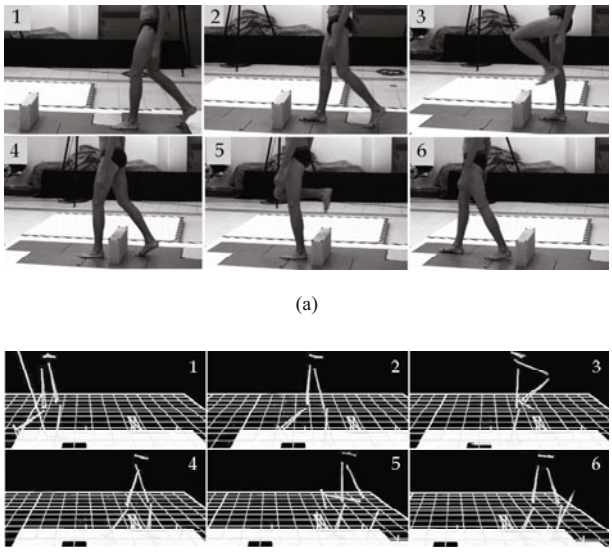

Fig. 4 Snapshots of an obstacle overcoming test: (a) a photo sequence; (b) a sequence of reconstructed lower body in Vicon Nexus software environment.

experimental process. After the treatment, position information of each marker can be outputted.

The second step is to reconstruct the experimental subject and its movement. This step is necessary because the system just can recognize separated markers and it cannot treat a set of makers as a waist, thighs, shanks or feet unless we specify them. Thus the purpose of this step is to assign the segments of the subject. To do this, first choose a name for a segment and then connect corresponding three markers sequentially to build the segment. Then the system will treat this segment as a rigid part and minor flutter among the three markers will be ignored. Coefficient of rigidity can be adjusted according to requirement. Fig. 4b shows a corresponding sequence of the reconstructed lower body obtained during post processing in Nexus software environment.

Based on the data acquired in the experiment, kinematics and ground reaction force of human walking are analyzed in section **3**. Furthermore, modeling and characterization of normal gait and obstacle overcoming gait are carried out in section **4**.

3 An analysis of obstacle overcoming

A sequence of both legs positions in Cartesian coordinate system is shown in Fig. 5a as referring to the experiment in Fig. 4, which have been modeled with

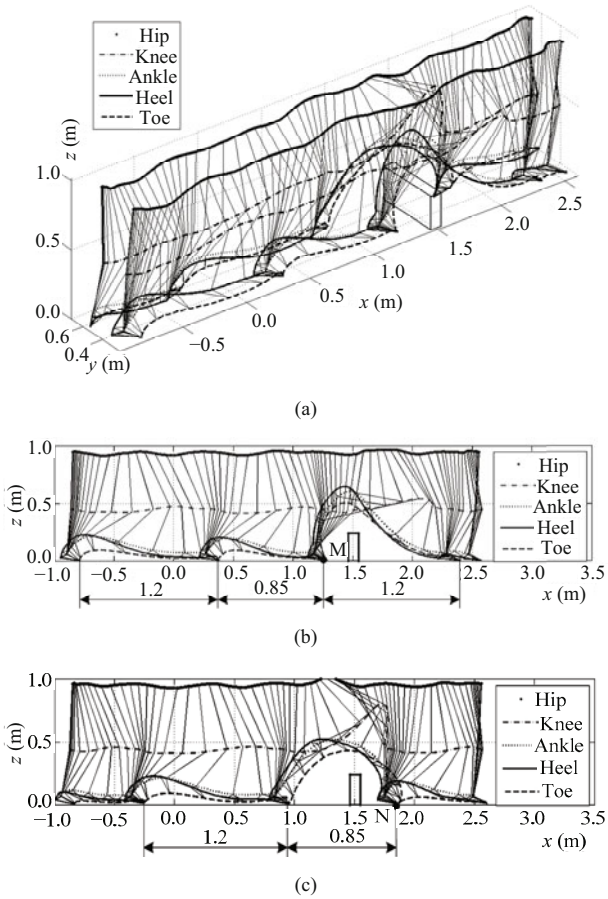

Fig. 5 Sequences of leg positions in Cartesian coordinates for the test in Fig. 4: (a) a 3-dimensional view; (b) projection of the right leg sequences in sagittal plane; (c) projection of the left leg sequences in sagittal plane.

post processing carried out in MATLAB environment. Each leg is drawn by connecting the 5 markers placed at the hip (marker 3 or 2), knee (marker 5 or 14), ankle (marker 8 or 17), heel (marker 10 or 19) and toe (marker 11 or 20) sequentially. In the experiment, a cuboid was placed at x=1.5 m as indicated in Fig. 5a. During the overcoming phase, the right step length was decreased in order to reach a suitable touchdown point M as shown in Fig. 5b, then the left leg overcame the cuboid first, and then the right leg overcame the cuboid. The step width is 0.2 m along y-axis. Stride length is approximately equal to 1.2 m before overcoming the cuboid, while overcoming the cuboid, both step length and step height were adjusted according to the size of the cuboid. In order to see clearly the features, legs movement and shapes of the walking gaits are illustrated separately as sequences of the right and left legs positions as in Fig. 5b and Fig. 5c.

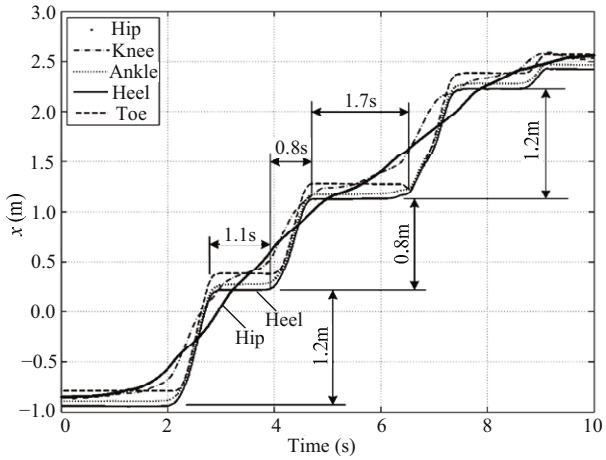

Fig. 6 *x*-coordinates of the five representative markers (markers 3, 5, 8, 10 and 11 in Fig. 2) of the right leg within the test in Fig. 4.

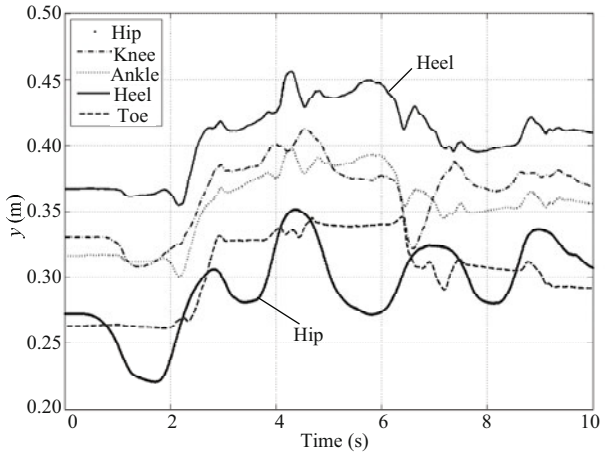

Fig. 7 *y*-coordinates of the five representative markers (markers 3, 5, 8, 10 and 11 in Fig. 2) of the right leg within the test in Fig. 4.

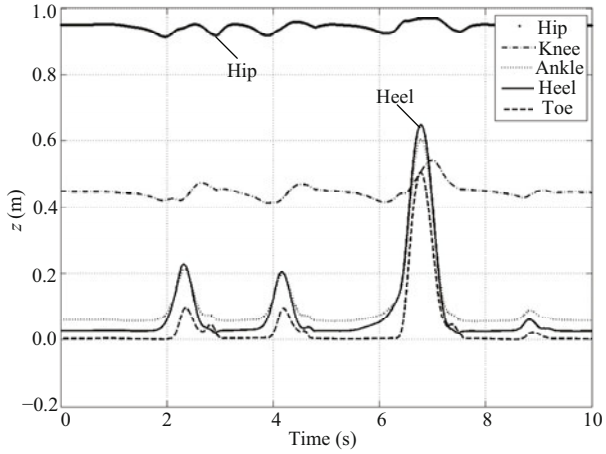

Fig. 8 *z*-coordinates of the five representative markers (markers 3, 5, 8, 10 and 11 in Fig. 2) of the right leg within the test in Fig. 4.

In Fig. 5b, stride length was decreased from 1.2 m to 0.85 m in front of the obstacle in order to reach a suitable touchdown point M. Then, as shown in Fig. 5c, after the left foot overpassed the top of the cuboid successfully, stride length was decreased immediately with the aim to avoid making the right foot an oversize stride length, which is the strategy for keeping balance. Sparse areas in the figures indicate that the legs move fast during swing phase, whereas compact areas depict that the legs move slowly during supporting phase, which is another strategy for keeping balance.

Figs. 6 to 8 show the *x*, *y*, and *z* coordinates of the five markers pasted at the hip (marker 3 in Fig. 2), knee (marker 5), ankle (marker 8), heel (marker 10) and toe (marker 11) points of the right leg. In particular, Fig. 6 shows the *x*-coordinate of the five markers. Curve of the hip marker indicates that the hip performs an approximate uniform motion in sagittal plane. Curves of the foot markers are step-shaped lines, of which the horizontal parts represent supporting phases and inclined parts represent swing phases. With a speed of about 0.4 $m \cdot s^{-1}$ during a test, supporting phase is longer than swing phase. This feature can be taken into account in dynamic walking control for humanoid robots.

In Fig. 7, *y*-coordinates of the five markers form periodic wavy curves with amplitude of about 0.1 m, which indicates that the lower body has a displacement of 0.1 m in transverse plane, namely human has lateral motion while walking with the aim to adjust the COG for keeping balance. As can be deduced from Fig. 8, the overcoming behavior of the right leg started at about 6.5 s and ended at 7.5 s. When the right leg was overcoming the cuboid, *z*-coordinate of the knee marker increased only a little, whereas *z*-coordinates of the ankle and heel markers surpassed the value of the knee marker. This means when overcoming obstacle, angular displacement of the knee joint is larger than that of the hip joint. Displacement of the hip in coronal plane is quite small, namely human upper body's COG varies very little in vertical direction, which indicates that human walking is quite smooth even when overcoming obstacle.

Fig. 9 shows the angle variations of the hip, knee and ankle joints of the right leg during the test in Fig. 4. The maximum angles of the right hip, knee, and ankle joints are about 102˚, 178˚ and 120˚, respectively and the minimum angles are about 58˚, 60˚ and 93˚, respectively. Similar values were recorded for the left leg joints. Obtained angle variations during experimental test can be used to guide the joint design of robotic legs. Moreover,

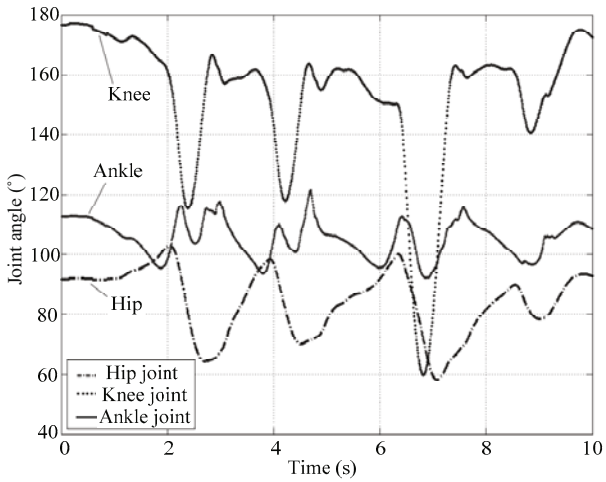

Fig. 9 Angle variation of the hip, knee, and ankle points of the right leg within the test in Fig. 4.

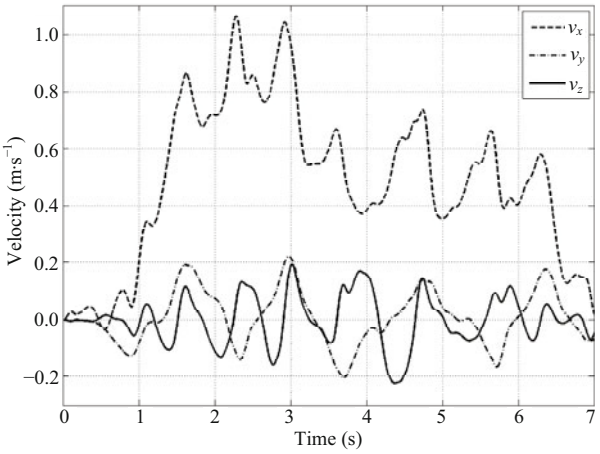

Fig. 10 Computed velocity of the left hip marker (marker 2 in Fig. 2) during obstacle overcoming test in Fig. 4, v_x: velocity along x-axis; v_y: velocity along y-axis; v_z: velocity along z-axis; x, y, z axes are the axes depicted in Fig. 5a.

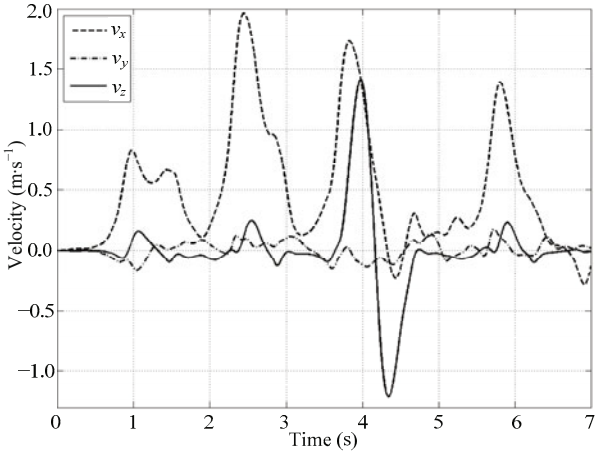

Fig. 11 Computed velocity of the left knee marker (marker 14 in Fig. 2) during obstacle overcoming test in Fig. 4, v_x: velocity along x-axis; v_y: velocity along y-axis; v_z: velocity along z-axis; x, y, z axes are the axes depicted in Fig. 5a.

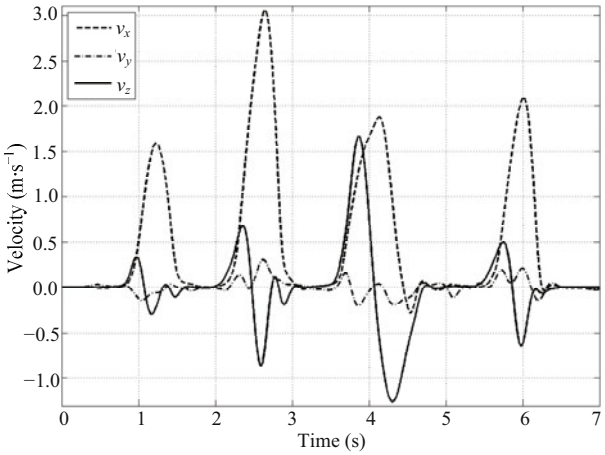

Fig. 12 Computed velocity of the left ankle marker (marker 17 in Fig. 2) during obstacle overcoming test in Fig. 4, v_x: velocity along x-axis; v_y: velocity along y-axis; v_z: velocity along z-axis; x, y, z axes are the axes depicted in Fig. 5a.

angular velocity and angular acceleration can be computed as the first and second derivatives of angular displacement.

Figs. 10 to 12 show the acquired velocities of the markers placed at the left hip (marker 2), knee (marker 14), and ankle (marker 17) points during the test in Fig. 4. In general, plots show that the hip has the lowest velocity whereas the ankle has the highest velocity. In addition, all the velocities show periodic feature. Amplitudes of the three velocities along x-axis, namely v_x, are approximately to 1.1 m·s^{-1}, 2 m·s^{-1}, and 3 m·s^{-1}, respectively. Furthermore, for each joint, velocity along the walking direction (in sagittal plane) is much larger than those in the other two directions (in coronal and transverse planes). Velocity along x-axis of the ankle marker shows that during each step, the acceleration phase and deceleration phase of the foot have a symmetry shape. From Fig. 10, it is observed that the phase of obstacle overcoming has a little impact to the upper body.

Figs. 13 to 15 show the accelerations of the three markers placed at the left hip (marker 2), knee (marker 14), and ankle (marker 17) joints during the test of overcoming obstacle. Plots show that the hip has the lowest acceleration whereas the ankle has the highest acceleration in average. Similarly to velocity, all the accelerations show periodic feature. Amplitudes of the three joints accelerations along x-axis are about 3.5 m·s^{-2}, 11 m·s^{-2}, and 22 m·s^{-2}, respectively. Velocity and acceleration of right hip, knee, and ankle joints are omitted here since they show similar features with the left ones.

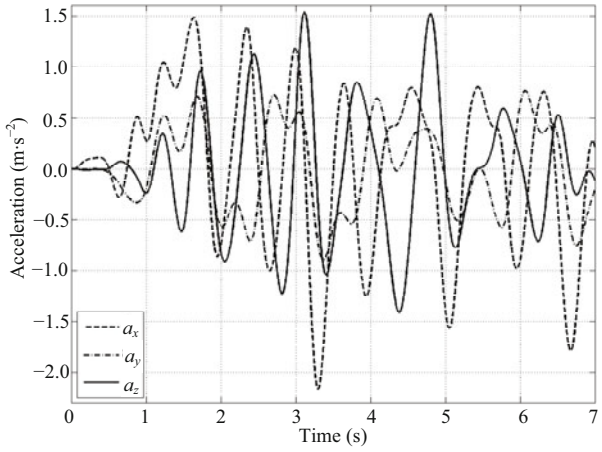

Fig. 13 Computed acceleration of the left hip marker (marker 2 in Fig. 2) during obstacle overcoming test in Fig. 4, a_x: acceleration along x-axis; a_y: acceleration along y-axis; a_z: acceleration along z-axis; x, y, z axes are the axes depicted in Fig. 5a.

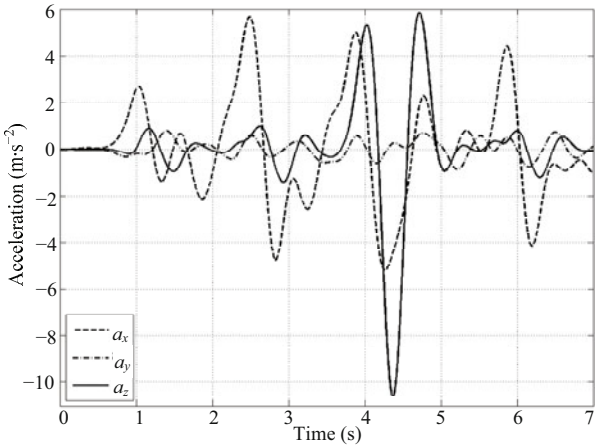

Fig. 14 Computed acceleration of the left knee marker (marker 14 in Fig. 2) during obstacle overcoming test in Fig. 4, a_x: acceleration along x-axis; a_y: acceleration along y-axis; a_z: acceleration along z-axis; x, y, z axes are the axes depicted in Fig. 5a.

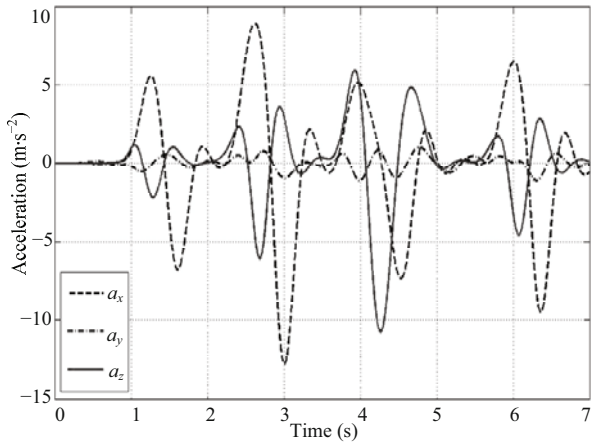

Fig. 15 Computed acceleration of the left ankle marker (marker 17 in Fig. 2) during obstacle overcoming test in Fig. 4, a_x: acceleration along x-axis; a_y: acceleration along y-axis; a_z: acceleration along z-axis; x, y, z axes are the axes depicted in Fig. 5a.

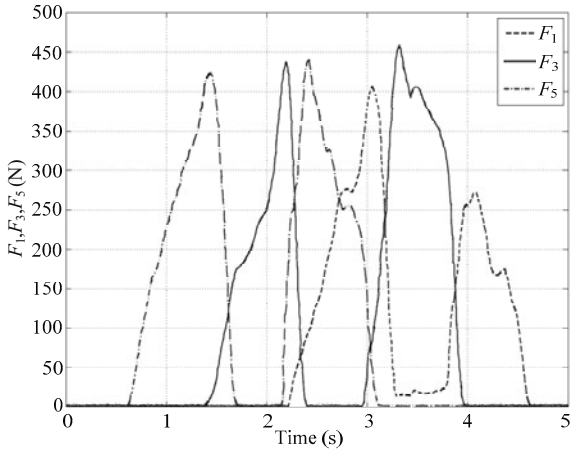

Fig. 16 Computed ground reaction force acting on right foot during straight walking test, F_1, F_3 and F_5 are the forces measured on force plates 1, 3 and 5, respectively.

Fig. 16 shows the acquired ground reaction force during the straight walking test. In particular, F_1, F_3, and F_5 are the forces exerting on right foot measured by force plates 1, 3, and 5, respectively (see Fig. 3). Within each curve, the first part is the force acting on the heel, while the second part is the force acting on the toe joint. Forces acting on the left foot are similar as those of the right foot.

4 An analysis and characterization of walking gaits

During the test of overcoming obstacle, there are two kinds of walking gaits, namely the normal gait, which was used before and after overcoming phase, and the adjusted gait, which was used during overcoming phase. Characteristics of these two types of walking gaits are analyzed according to the trajectories of the six markers which are pasted at the ankles (markers 8 and 17), heels (markers 10 and 19) and toes (markers 11 and 20) points of the two feet as shown in Fig. 2.

Fig. 17 shows the trajectories of the three markers that were placed at the left ankle (marker 17), heel (marker 19), and toe (marker 20) joints of normal gait. Walking direction shown in the figure is from the right side to the left side. As illustrated in heel trajectory, the foot rotates around the toe joint for an angle θ during toe-off phase, which lift the COG with the aim to use gravity to provide propulsion for the coming swing phase. This verifies that human can make use of gravity effectively during walking. During swing phase, the foot rotates around the moving knee joint. Since knee moves

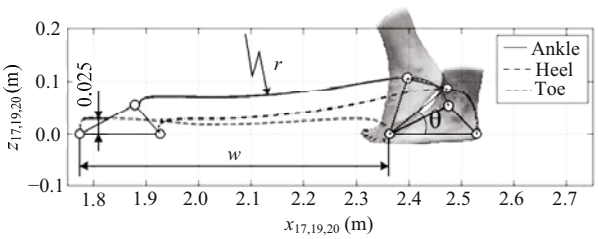

Fig. 17 Trajectories of the markers (17, 19, and 20 as in Fig. 2) placed on left foot for normal gait, r: curvature of the ankle trajectory; w: step length; θ: rotation angel around the toe joint.

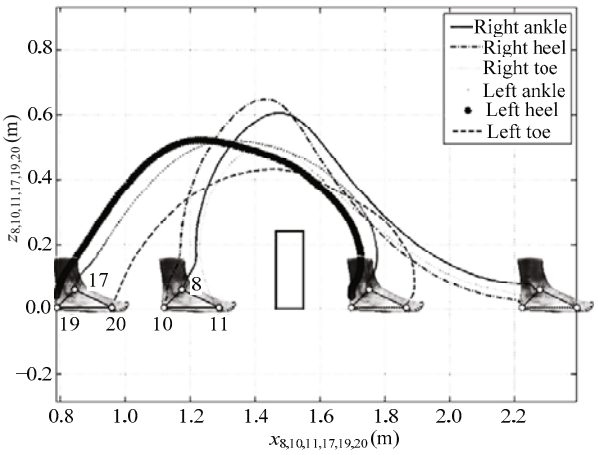

(a)

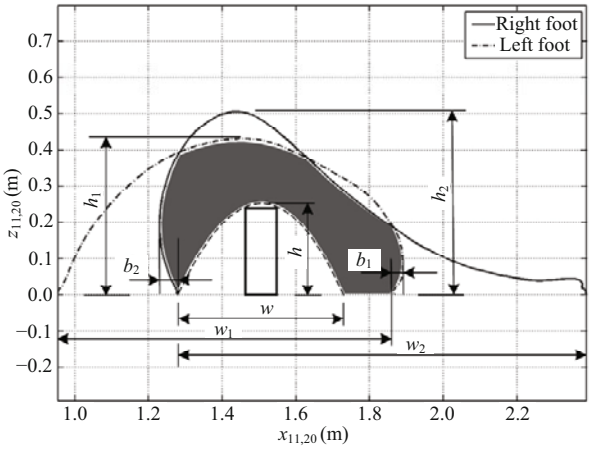

(b)

Fig. 18 Modeling of the foot trajectories during the obstacle overcoming test in Fig. 4.

forward along with the foot, trajectory of the foot has a very small curvature. In addition, during swing phase the toe moves very near the ground, which makes the foot has very small impact force when striking the ground.

Fig. 18 shows the trajectories of the six markers that were placed at the ankles, heels, and toes of the two feet during obstacle overcoming phase, respectively. When analyzing the adjusted gait for obstacle overcoming, the foot gesture is omitted and only the toe trajectories are extracted from Fig. 18a as to be shown in Fig. 18b.

In Fig. 18b, black dashed line represents the minimal size of the gait that needs to be guaranteed for overcoming the obstacle successfully, of which w and h are the step length and height, respectively. When referring to a specified obstacle, h and w are fixed. w_1, h_1, w_2, and h_2 are the step length and height of the left and right feet, respectively. b_1 and b_2 are the back motion of the left and right feet, respectively. The shadow area, which is mainly identified by b_1, b_2, h_1, h, and w, is defined as security domain. Security domain is used for evaluating motion stability and efficiency of biped robots, and it is a proportional result of walking stability and velocity. In particular, increase b_1 and b_2 will decrease the step length, which could enhance the walking stability, meanwhile the foot is more near the obstacle, and thus the subject should be more careful to overcome the obstacle, which will decrease the walking velocity, and vice versa. Thus in gait planning of overcoming obstacle, a security domain determined by suitable values of gait dimensions could benefit both the walking stability and walking velocity.

5 Conclusion

This paper introduced a fairly easy way to study human behavior in overcoming obstacle with a motion capture system. The experimental design and configuration have such advantages as it is easy to implement, it has no limitation to the experimental subject so that the subject can perform natural locomotion, it has high accuracy in the data acquisition, and it can measure plenty information all at once. By this simple experiment, we obtained much information of displacement, angle variation, velocity, acceleration, ground reaction force, trajectory and walking gait. Experimental results show that human locomotion is approximately symmetric, periodic and smooth, and show that human locomotion can make use of gravity effectively. In addition, by analyzing the experimental outputs, the reasons which lead to smooth walking can be identified as that human upper body's COG has slight movement in the vertical direction during walking, and as that toes move very near to the ground in swing phase; the reason which makes human locomotion use gravity effectively can be identified as that feet rotate around the toe joints during

toe-off phase aiming at using gravitational potential energy to provide propulsion for swing phase. Furthermore, both normal walking gait and obstacle overcoming gait have been characterized in a form that can provide necessary knowledge and useful databases for the implementation of motion planning and gait planning towards overcoming obstacle for humanoid robots. Besides, researchers can easily transfer the way to other kind of study of human locomotion like for examples straight walking, changing direction and ascending/descending stairs.

References

[1] Faure F, Debunne G, Cani-Gascuel M P, Multon F. Dynamic analysis of human walking. *Proceedings of the Eurographics Workshop on Computer Animation and Simulation*, Budapest, Hungary, 1997, 53–65.

[2] Öberg T. Motion analysis in clinical biomechanics. *Biomechanics of Musculoskeletal System-Medical Robotics*, Polish Academy of Science, Warsaw, 2000.

[3] Adrian M, Cooper J. *Biomechanics of Human Movement*, Benchmark Press, Indianapolis, 1995.

[4] Luo X, Xu W L. Planning and control for passive dynamics based walking of 3D biped robots. *Journal of Bionic Engineering*, 2012, **9**, 143–155.

[5] Koeda M, Ito T, Yoshikawa T. Shuffle turning in humanoid robots through load distribution control of the soles. *Robotica*, 2011, **29**, 1017–1024.

[6] Kim J Y, Park I W, Oh J H. Realization of dynamic stair climbing for biped humanoid robot using force/torque sensors. *Journal of Intelligent and Robotic Systems*, 2009, **56**, 389–423.

[7] Guan Y S, Yokoi K, Tanie K. Feasibility: Can humanoid robots overcome given obstacles? *Proceedings of the IEEE International Conference on Robotics and Automation*, Barcelona, Spain, 2005, 1054–1059.

[8] Verrelst B, Stasse O, Yokoi K, Vanderborght B. Dynamically stepping over obstacles by the humanoid robot HRP-2. *Proceedings of the* 6*th IEEE-RAS International Conference on Humanoid Robots*, Genova, Italy, 2006, 117–123.

[9] Chiang M H, Chang F R. Anthropomorphic design of the human-like walking robot. *Journal of Bionic Engineering*, 2013, **10**, 186–193.

[10] Qian K, Ma X D, Dai X Z, Fang F. Robotic etiquette: Socially acceptable navigation of service robots with human motion pattern learning and prediction. *Journal of Bionic Engineering*, 2010, **7**, 150–160.

[11] Ottaviano E, Ceccarelli M, Palmucci F. An application of CaTraSys, a cable-based parallel measuring system for an experimental characterization of human walking. *Robotica*, 2010, **28**, 119–133.

[12] Boutin L, Eon A, Zeghloul S, Lacouture P. An auto-adaptable algorithm to generate human-like locomotion for different humanoid robots based on motion capture data. *Proceedings of International Conference on Intelligent Robots and Systems* (*IROS*), Taipei, China, 2010, 1256–1261.

[13] Boutin L, Eon A, Zeghloul S, Lacouture P. From human motion capture to humanoid locomotion imitation application to the robots HRP-2 and HOAP-3. *Robotica*, 2011, **29**, 325–334.

[14] Draganich L F, Kuo C E. The effects of walking speed on obstacle crossing in healthy young and healthy older adults. *Journal of Biomechanical Engineering*, 2004, **37**, 889–896.

[15] Krell J, Patla A E. The influence of multiple obstacles in the travel path on avoidance strategy. *Gait Posture*, 2002, **16**, 15–19.

[16] Chou L S, Kaufman K R, Brey R H, Draganich L F. Motion of the whole body's center of mass when stepping over obstacles of different heights. *Gait Posture*, 2001, **13**, 17–26.

[17] Lowrey C R, Watson A, Vallis L A. Age-related changes in avoidance strategies when negotiating single and multiple obstacles. *Experimental Brain Research*, 2007, **182**, 289–299.

[18] Patla A E, Vickers J N. Where and when do we look as we approach and step over an obstacle in the travel path? *Neuroreport*, 1997, **8**, 3661–3665.

[19] Patla A E, Greig M. Anyway you look at it successful obstacle negotiation needs visually guided on-line foot placement regulation during the approach phase. *Neuroscience Letters*, 2006, **397**, 110–114.

[20] MacLellan M J, Patla A E. Stepping over an obstacle on a compliant travel surface reveals adaptive and maladaptive changes in locomotion patterns. *Experimental Brain Research*, 2006, **173**, 531–538.

[21] *Vicon Nexus*, [2013-12-16], http://www.vicon.com